ARTICLE

Supporting Information for

In situ growth of metal–organic frameworks in nanochannels for highly sensitive microcystin-LR detection†

Wei-Qi Zhang,[†a] Yi-Dan Tu,[†a] Xu-Gang Wang,[a] Yu Huang,*[ab] and Fan Xia [ab]

[a] *State Key Laboratory of Biogeology and Environmental Geology, Engineering Research Center of Nano-Geomaterials of Ministry of Education, Faculty of Material Science and Chemistry, China University of Geosciences, Wuhan 430074, P. R. China.*

[b] *Zhejiang Institute, China University of Geosciences, Hangzhou, 311305, China*

† These authors contributed equally to this work.

* Corresponding author: Y. Huang

E-mail: yuhuang@cug.edu.cn;

Synergistic effect of nanochannels

In order to explore the synergistic effect of DNA@MOFs-AAO nanochannels, the general ionic conductance model was used to calculate the ion current. Due to the voltage drive, the ions in the solution pass through the nanochannels and form an open-circuit current signal when a voltage is applied to both ends of the nanochannels filled with the electrolyte solution. Based on the universal ionic conductance model of cylindrical nanochannels, the ionic current I of the nanochannels can finally be derived into the following equation:

$$I = V\left([n_+\mu_+ + n_-\mu_-]e\right)\left(\frac{4h}{\pi D^2} + \frac{1}{D}\right)^{-1} + \frac{V\mu_{\oplus}\pi D\sigma}{h} \quad (1)$$

V is the applied voltage; D is the diameter of the cylindrical nanochannels, which regarded as an effective diameter; h is the length of the nanochannels, n_+ and n_- represent the density of positive and negative ions, respectively; μ_+ and μ_- represent the electrophoretic mobility of positive and negative ions, respectively; e is the elementary charge. The last term of the equation (1) ($V\mu_{\oplus}\Pi D\sigma/h$) represents the transport of ions through the surface with a highly charged pore; $\mu_{\oplus}$ represents the solution mobility of counterions adsorbed on the charged pore, with a surface charge density of σ (as opposed to the sign of the counter ion charge). Because the h of the membrane involved in this experiment is much larger than D. Therefore, the term $1/D$ of the access resistance in equation (1) can be ignored. In addition, the electrolytes used in this experiment were 0.1 M KCl. The first term in equation (1) ($[n_+\mu_+ + n_-\mu_-]$) can also be ignored. Therefore, equation (1) can be expressed as:

$$I = V\left(\frac{4h}{\pi D^2}\right)^{-1} + \frac{V\mu_{\oplus}\pi D\sigma}{h} \quad (2)$$

When the concentration of electrolyte is greater than 0.1 M, the transport of ions in the nanochannels is mainly determined by the diffusion and migration kinetics of ions. In this case, the charge properties of the nanochannels wall do not have significant effect on the transport of ions. In this experiment, the concentration of electrolyte is 0.1 M KCl, so the last term in equation (2) ($V\mu_{\oplus}\Pi D\sigma/h$) can be ignored. The ionic current of the nanochannels can be further simplified to:

$$I = V\left(\frac{4h}{\pi D^2}\right)^{-1} \quad (3)$$

Through equation (3), the ionic current of the nanochannels was mainly determined by its effective diameter (D) in this experiment. Taking into account this understanding, the changes of ionic current and effective diameter were studied carefully in the content.

As shown in Fig. 8A, the AAO which activates the hydroxyl group and connects the aldehyde group, the nanochannels after the modified probes were blocked by the stretched probes (closed state), with effective diameters of *d* and *d'* for DNA@AAO and DNA@MOFs-AAO, respectively. When the nanochannels sensing and selectively binding MC-LR, the probes folded. The effective diameter of the nanochannels increased as a result. Here, we assumed that the increase of the effective diameter of the probes binding targets were the same as *Δd* for the two kinds of nanochannels of DNA@AAO and DNA@MOFs-AAO. Therefore, the nanochannels were in an open state after binding with MC-LR, and the effective diameters of DNA@AAO and DNA@MOF were $d+\Delta d$ and $d'+\Delta d$, respectively. In this experiment, the increase of ionic current was defined as R_I for DNA@AAO and R_I' for DNA@MOFs-AAO:

$$R_I = \frac{I_2 - I_1}{I_1} \tag{4}$$

$$R_I' = \frac{I_2' - I_1'}{I_1'} \tag{5}$$

I_1 and I_2 represent the ionic current of nanochannels with DNA@AAO before and after binding the MC-LR, respectively. I_1' and I_2' represent the ionic current of nanochannels with DNA@MOFs-AAO before and after binding the MC-LR, respectively. According to equation (3), I_1 is $(Vd^2/4h)$ and I_2 is $(V(d+\Delta d)^2/4h)$; I_1' is $(Vd'^2/4h)$ and I_2' is $(V(d'+\Delta d)^2/4h)$. So, equation (4) and equation (5) can be written as:

$$R_I = \frac{\frac{V\pi(d+\Delta d)^2}{4h} - \frac{V\pi d^2}{4h}}{\frac{V\pi d^2}{4h}} = \frac{2d\Delta d + \Delta d^2}{d^2} \tag{6}$$

$$R_I' = \frac{\frac{V\pi(d'+\Delta d)^2}{4h} - \frac{V\pi d'^2}{4h}}{\frac{V\pi d'^2}{4h}} = \frac{2d'\Delta d + \Delta d^2}{d'^2} \tag{7}$$

To compare the ionic current increasement of nanochannels with DNA@AAO and DNA@MOFs-AAO before and after binding the MC-LR, the difference between R_I' and R_I was calculated:

$$R_I' - R_I = \frac{2d\Delta d + \Delta d^2}{d^2} - \frac{2d'\Delta d + \Delta d^2}{d'^2} = \frac{\Delta d^2(d^2 - d'^2)}{d^2 d'^2} + \frac{2\Delta d(d - d')}{dd'} \tag{8}$$

Finally, the simplified formula is shown above.

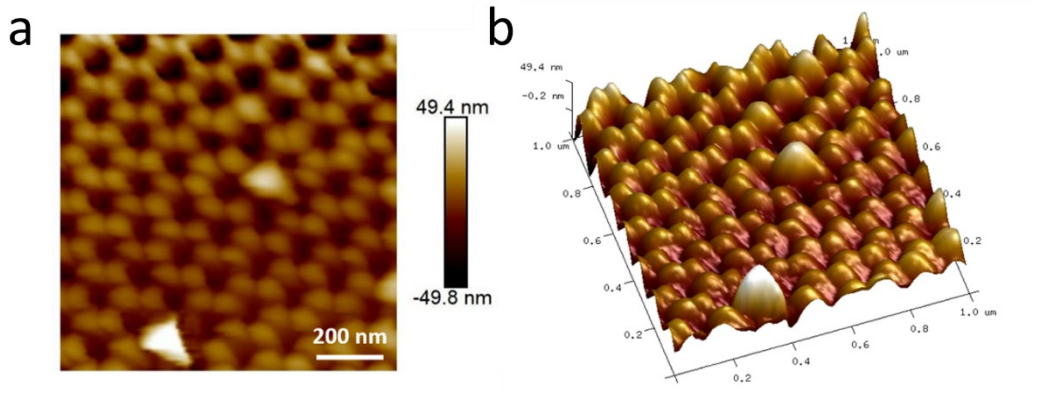

Figure S1. Surface morphology of DNA@AAO characterized by AFM. (a) 2D AFM image. (b) 3D AFM image.

Table S1. The performance of different analysis methods for MC-LR detection in recency years.

Sensor Platform	Linear range (ng/mL)	LOD (ng/mL)	Recovery (%)	Samples	Year	Refs
3D graphene based electrode	0.05-20	0.05	92.7	water	2017	[1]
AgNP-Nafion-xGnP	0.5-5000	0.017	105.8	seawater	2017	[2]
PPBI	0.1-100	0.012	95.2-110	water	2018	[3]
GNS@SiO_2	0.01-100	0.014	100-107	lake water	2019	[4]
AuNPs@MOF	0.05-75000	0.02	102.4	water	2019	[5]
MGNnP-PEI	0.1-500	0.053	98.2-101.7	fresh water lagoon	2020	[6]
TAM-C5 Q-body	-	0.45	94.8−120.0	river water	2021	[7]
DNA@MOF-AAO	0.1-1000	0.004	93.9-106.7	lake water/tap water	2022	This study

References

[1] W. Zhang, C. Han, B. Jia, C. Saint, M. Nadagouda, P. Falaras, L. Sygellou, V. Vogiazi, D.D. Dionysiou, A 3D graphene-based biosensor as an early microcystin-LR screening tool in sources of drinking water supply, Electrochimica Acta, 236 (2017) 319-327.

[2] N. Zanato, L. Talamini, T.R. Silva, I.C. Vieira, Microcystin-LR label-free immunosensor based on exfoliated graphite nanoplatelets and silver nanoparticles, Talanta, 175 (2017) 38-45.

[3] J. Wu, Y. Xianyu, X. Wang, D. Hu, Z. Zhao, N. Lu, M. Xie, H. Lei, Y. Chen, Enzyme-Free Amplification Strategy for Biosensing Using Fe3+–Poly(glutamic acid) Coordination Chemistry, Analytical Chemistry, 90 (2018) 4725-4732.

[4] M. Li, S.K. Paidi, E. Sakowski, S. Preheim, I. Barman, Ultrasensitive Detection of Hepatotoxic Microcystin Production from Cyanobacteria Using Surface-Enhanced Raman Scattering Immunosensor, ACS Sensors, 4 (2019) 1203-1210.

[5] K. Zhang, K. Dai, R. Bai, Y. Ma, Y. Deng, D. Li, X. Zhang, R. Hu, Y. Yang, A competitive microcystin-LR immunosensor based on Au NPs@metal-organic framework (MIL-101), Chinese Chemical Letters, 30 (2019) 664-667.

[6] R. Almeida de Oliveira, N. Zanato, I. Cruz Vieira, Label-free Immunosensor for the Determination of Microcystin-LR in Water, Electroanalysis, 32 (2020) 2166-2173.

[7] L. Zhang, H. Dong, H. Li, B. Li, G. Zhao, H. Cai, L. Chen, J. Dong, Novel signal-on immunosensors for rapid and sensitive detection of Microcystin-LR, Microchemical Journal, 167 (2021) 106295.